DIGITAL ACCESS TO SCHOLARSHIP AT HARVARD
DASH.HARVARD.EDU

HARVARD LIBRARY
Office for Scholarly Communication

H2CO and N2H+ in Protoplanetary Disks: Evidence for a CO-Ice Regulated Chemistry

The Harvard community has made this article openly available. **Please share** how this access benefits you. Your story matters

Citation	Qi, Chunhua, Karin I. Öberg, and David J. Wilner. 2013. "H2CO AND N2H+IN PROTOPLANETARY DISKS: EVIDENCE FOR A CO-ICE REGULATED CHEMISTRY." The Astrophysical Journal 765 (1) (February 13): 34. doi:10.1088/0004-637x/765/1/34.
Published Version	doi:10.1088/0004-637X/765/1/34
Citable link	http://nrs.harvard.edu/urn-3:HUL.InstRepos:33946923
Terms of Use	This article was downloaded from Harvard University's DASH repository, and is made available under the terms and conditions applicable to Open Access Policy Articles, as set forth at http://nrs.harvard.edu/urn-3:HUL.InstRepos:dash.current.terms-of-use#OAP

H$_2$CO and N$_2$H$^+$ in Protoplanetary Disks: Evidence for a CO-ice Regulated Chemistry

Chunhua Qi

Harvard-Smithsonian Center for Astrophysics, 60 Garden Street, Cambridge, MA 02138, USA

and

Karin I. Öberg

University of Virginia, Departments of Chemistry and Astronomy, Charlottesville, VA 22904, USA

and

David J. Wilner

Harvard-Smithsonian Center for Astrophysics, 60 Garden Street, Cambridge, MA 02138, USA

ABSTRACT

We present Submillimeter Array observations of H_2CO and N_2H^+ emission in the disks around the T Tauri star TW Hya and the Herbig Ae star HD 163296 at $2''$–$6''$ resolution and discuss the distribution of these species with respect to CO freeze-out. The H_2CO and N_2H^+ emission toward HD 163296 does not peak at the continuum emission center that marks the stellar position but is instead significantly offset. Using a previously developed model for the physical structure of this disk, we show that the H_2CO observations are reproduced if H_2CO is present predominantly in the cold outer disk regions. A model where H_2CO is present only beyond the CO snow line (estimated at a radius of 160 AU) matches the observations well. We also show that the average H_2CO excitation temperature, calculated from two transitions of H_2CO observed in these two disks and a larger sample of disks around T Tauri stars in the DISCS (the Disk Imaging Survey of Chemistry with SMA) program, is consistent with the CO freeze-out temperature of $\sim$20 K. In addition, we show that N_2H^+ and H_2CO line fluxes in disks are strongly correlated, indicative of co-formation of these species across the sample. Taken together, these results imply that H_2CO and N_2H^+ are generally present in disks only at low temperatures where CO depletes onto grains, consistent with fast destruction of N_2H^+ by gas-phase CO, and *in situ* formation of H_2CO through hydrogenation of CO ice. In this scenario H_2CO, CH_3OH and N_2H^+ emission in disks should appear as rings with the inner edge at the CO midplane snow line. This prediction can be tested directly using observations from ALMA with higher resolution and better sensitivity.

Subject headings: protoplanetary disks; astrochemistry; stars: formation; ISM: molecules; techniques: high angular resolution; radio lines: ISM

1. Introduction

Planetary systems are assembled from dust and gas in the disks surrounding pre-main sequence stars. The nature of the formed planets are intimately linked to the structure, composition and evolution of the parent circumstellar disk. Molecular emission lines serve as probes of disk characteristics, such as density, temperature and ionization fraction, that are not accessible by other observations. For example, N_2H^+ along with the deuterated ions like H_2D^+ and DCO^+ are believed to trace the ionization fraction near the midplane of the disks (Öberg et al. 2011c). Molecular distributions in disks are also important to characterize because of their connection with the composition of forming planetesimals. This especially true of organic molecules, of which H_2CO is an important representative. While most molecules are expected to be reprocessed in larger planetary bodies, the disk-chemical composition may survive quite intact in icy planetesimals, including comets (Mumma & Charnley 2011). Such planetesimals may have seeded the Earth with water and organics, connecting disk chemistry with the origins of life. Predicting the organic composition of these planetesimals depend on our understanding of the distribution of the organic composition of grains in the disks.

The overall disk chemical structure is set by a combination of photochemistry at the disk surface and sequential freeze-out of molecules in the disk interior (e.g. Aikawa et al. 2002). The distributions of N_2H^+ and H_2CO and their relationship to CO present important test cases of the chemical models. The CO molecule is one of the last to freeze out and predicted to deplete quickly from the gas-phase at T$< 20 - 25$ K for typical disk mid-plane densities. Abundant N_2H^+ is expected only where CO is depleted because N_2H^+ forms from protonation of N_2, which remains in the gas-phase at temperatures a few degrees lower than CO (Öberg et al. 2005), and is destroyed mainly by reactions with CO (Bergin et al. 2002). In dense cores in star forming regions, the abundance of CO is observed to show a strong

anti-correlation with N_2H^+ (e.g. Caselli et al. 1999; Bergin et al. 2002; Jørgensen 2004). In disk models, this effect is manifested as a jump in the N_2H^+ column density at the CO "snow line", one order of magnitude in a recent calculation (Walsh et al. 2012). The snow line is here defined as the disk radius where the midplane dust temperature is cold enough for volatiles to condense into ice grains.

The H_2CO chemistry is more complicated than N_2H^+ because H_2CO can form through several different pathways, both in the gas-phase and on grain-surfaces. Grain-surface formation of H_2CO should depend directly on CO freeze-out; constrained by theory (Tielens & Hagen 1982; Cuppen et al. 2009) and experiments (e.g. Watanabe et al. 2003; Fuchs et al. 2009), H_2CO (and CH_3OH) form readily from CO ice hydrogenation. If this is the dominant formation pathway of H_2CO in disks, and if ices are partially desorbed non-thermally (e.g. Garrod et al. 2007; Öberg et al. 2009b,a), then H_2CO gas should coincide with N_2H^+ exterior to the CO snow line.

To date, emission from millimeter wavelength H_2CO and N_2H^+ lines has been detected toward 8 and 6 protoplanetary disks, respectively (Dutrey et al. 1997; Aikawa et al. 2003; Qi et al. 2003; Thi et al. 2004; Dutrey et al. 2007; Henning & Semenov 2008; Öberg et al. 2010, 2011b). Most detections are toward T Tauri stars with massive disks, and the detection fraction toward more luminous Herbig Ae stars is low (Öberg et al. 2011b). Based on these observations, H_2CO and N_2H^+ are mainly abundant in disks with large reservoirs of cold dust and gas, where CO freeze-out is expected to occur. A direct connection between CO freeze-out and N_2H^+ and H_2CO in disks has yet to be observationally established, however.

In this paper we present Submillimeter Array (SMA) observations of H_2CO and N_2H^+ toward the disks around HD 163296 and TW Hya, and we use these new observations along with H_2CO and N_2H^+ observations from DISCS (Disk Imaging Survey of Chemistry with

SMA) to constrain the H_2CO and N_2H^+ distributions. The new data and their calibration are described in §2. In §3, we present the H_2CO and N_2H^+ images and spectra toward HD 163296 and TW Hya, models of the H_2CO distribution toward HD 163296, H_2CO excitation temperature calculations, and examine the relationship between H_2CO and N_2H^+ emission across the sample of disks. In §4, we discuss the implications of these results, summarize the mounting evidence for CO-ice regulated chemistry and make predictions for future observations of H_2CO and N_2H^+ emission from disks with better sensitivity and resolution.

2. Observations

The observations of HD 163296 (R.A. = $17^h56^m21.279^s$, decl. = $-21°57'22''.38$; J2000.0) were made between 2008 and 2012, and of TW Hydrae (R.A. = $11^h01^m51.875^s$, decl. = $-34°42'17''.155$; J2000.0) between 2008 and 2012, using the eight-antenna Submillimeter Array (SMA) located atop Mauna Kea, Hawaii. Table 1 provides a summary of the observational parameters and results. For the 2007 and 2008 observations, the SMA receivers operated in a double-sideband mode with an intermediate frequency (IF) band of 4–6 GHz from the local oscillator frequency, sent over fiber optic transmission lines to 24 overlapping "chunks" of the digital correlator. The 2012 observations were made after an upgrade that enabled a second IF band of 6–8 GHz, effectively doubling the bandwidth.

The SMA observations of HD 163296 were carried out in the compact-north (COM-N), compact (COM) and subcompact (SUB) array configurations. The 2007 observations included the DCO^+ 3–2 line at 216.1126 GHz and the H_2CO $3_{1,2} - 2_{1,1}$ line at 225.698 GHz. The 2012 observations included the N_2H^+ 3–2 at 279.512 GHz and the H_2CO $4_{1,4} - 3_{1,3}$ line at 281.527 GHz. The observing loops used J1733–130 as the main gain calibrator and observed J1744–312 every other cycle to check the phase calibration. Flux calibration was

done using observations of Titan and Uranus. The derived fluxes of J1733-130 were 1.19 Jy (2007 Mar 20), 1.25 Jy (2012 Jun 10), 1.40 Jy (2012 Aug 12 and 14). The bandpass response was calibrated using observations of 3C279, Uranus and J1924–292.

The SMA observations of TW Hya were carried out in the compact (COM) and subcompact (SUB) array configurations. The 2008 observations included the H_2CO $5_{1,5} - 4_{1,4}$ line at 351.769 GHz. The 2012 Jan 13 SUB observation included the H_2CO $4_{1,4} - 3_{1,3}$ and N_2H^+ 3–2 lines, like HD 163296, but unfortunately the chunk containing N_2H^+ was corrupted and unusable. The 2012 Jun 04 COM observation using a similar setting successfully included the N_2H^+ line. The observing loops used J1037–295 as the gain calibrator. Flux calibration was done using observations of Titan and Callisto. The derived fluxes of J1037–295 were 0.73 Jy (2008 Feb 23), 0.73 Jy (2012 Jan 13) and 0.82 Jy (2012 Jun 4). The bandpass response was calibrated using observations of 3C279 and 3C273.

Routine calibration tasks were performed using the MIR software package [1], and imaging and deconvolution were accomplished in the MIRIAD software package.

3. Results

In this section we present detections of H_2CO and N_2H^+ emission lines toward HD 163296 and TW Hya, display their respective distributions (§3.1), and compare the higher quality observations of H_2CO in HD 163296 with models (§3.2). We then combine the new data with previously reported H_2CO and N_2H^+ detections in disks to examine trends with respect to H_2CO excitation temperature (§3.3) and with each other (§3.4).

---

[1]http://www.cfa.harvard.edu/∼cqi/mircook.html

3.1. H_2CO and N_2H^+ towards HD 163296 and TW Hya

Figure 1 shows images of the spectrally integrated emission toward TW Hya and HD 163296 at the rest frequencies of two H_2CO lines and the N_2H^+ $J = 3 - 2$ line. H_2CO $4_{1,4} - 3_{1,3}$ and $5_{1,5} - 4_{1,4}$ and N_2H^+ are detected toward TW Hya, and H_2CO $3_{1,2} - 2_{1,1}$ and H_2CO $4_{1,4} - 3_{1,3}$ and N_2H^+ are detected toward HD 163296. The emission toward TW Hya appears to be centrally peaked at the size scale of the beams (FWHM $> 2''$).

Toward HD 163296, however, neither the H_2CO lines nor the N_2H^+ line emission peaks at the location of the continuum peak that marks the stellar position, but instead show significant offsets. This is most readily apparent for the H_2CO $3_{1,2} - 2_{1,1}$ line that was observed with a slightly smaller and more advantageously rotated beam, where the emission appears ring-like. This is the second reported observation of a ring-like H_2CO distribution after DM Tau (Henning & Semenov 2008). Interpreting the H_2CO emission toward DM Tau is however complicated by a large central cavity in dust emission (Andrews et al. 2011).

Figure 2 shows the spatially integrated spectra. The line shapes and central velocities agree with what has been previously observed for other molecular lines toward these disks. The line fluxes are listed in Table 1, and the values are comparable to detections of these lines toward other large protoplanetary disks (Öberg et al. 2010, 2011b).

3.2.   HD 163296 H_2CO Model Results

Figure 1 demonstrates that H_2CO emission toward HD 163296 is spatially resolved and thus contains information on the radial distribution of H_2CO in the disk. The relative excitation of the two H_2CO transitions should probe primarily the vertical distribution and thus provide complementary constraints. We explore the H_2CO distribution based on a previously developed accretion disk model with a well-defined temperature and density

structure, constrained by the HD 163296 broadband spectral energy distribution, spatially resolved millimeter dust continuum, and multiple CO and CO isotopologue line observations (Qi et al. 2011). We adopt the same methods as Qi et al. (2008) for constraining the H_2CO distribution, here fitting models that assume a radial power-law (§3.2.1) and a simple ring with inner boundary at the CO "snow line" (§3.2.2).

3.2.1. Power-law Model

For a first-order analysis of the distribution of H_2CO, we model the radial variation in the column density as a power law $N_{100} \times (r/100)^p$ between an inner radius R_{in} and outer radius R_{out}, where N_{100} is the column density at 100 AU in cm^{-2}, r is the distance from the star in AU, and p is the power-law index.

For the vertical distribution, we assume that H_2CO is present with a constant abundance in a layer with boundaries toward the midplane and toward the surface of the disk (similar to Qi et al. (2008)). This assumption is motivated by chemical models (e.g. Aikawa & Nomura 2006) that predict a three-layered structure where most molecules are photodissociated in the surface layer, frozen out in the midplane, and have an abundance that peaks at intermediate disk heights. The surface (σ_s) and midplane (σ_m) boundaries are presented in terms of $\Sigma_{21} = \Sigma_H/(1.59 \times 10^{21} cm^{-2})$, where Σ_H is the hydrogen column density measured from the disk surface. This simple model approximates the vertical location where H_2CO is most abundant. The excitation of multiple transitions can constrain both σ_s and σ_m, but in this case of very modest signal-to-noise, we fix σ_s to 0.79, the surface boundary found for CO by Qi et al. (2011), and we fit σ_m for the midplane boundary and the power-law parameters (N_{100}, p, R_{in} and R_{out}).

Using the structure model, we compute a grid of synthetic H_2CO visibility datasets

over a range of R_{out}, R_{in}, p, σ_m and N_{100} values and compare with the observations. The best-fit model is obtained by minimizing χ^2, the weighted difference between the real and imaginary part of the complex visibility measured in the (u, v)-plane sampled by the SMA observations of both H_2CO transitions. We use the two-dimensional Monte Carlo model RATRAN (Hogerheijde & van der Tak 2000) to calculate the radiative transfer and molecular excitation. The collisional rates are taken from the Leiden Atomic and Molecular Database (Schöier et al. 2005).

Table 2 lists the best-fit parameters of the model. The power-law index of 2 implies an H_2CO column density that strongly increases with radius. Figure 3 shows the best-fit radial distribution of the H_2CO column density. Figures 4 and 5 present comparisons between the observed channel maps and the best-fit model. The model reproduces the main features of the observations remarkably well, in particular the flux ratio between the inner and outer channels, and the lack of emission at the location of the continuum peak.

Figure 6 shows the χ^2 surfaces for the R_{in} and R_{out} versus the power law index p, which enables us to quantify the uncertainties associated with the inner and outer region sizes and the power-law index. We find that p is constrained between 0.5–3.0 (within 1σ) while R_{in} is constrained to be <200 AU. The χ^2 value does not change significantly for inner radii <90 AU, as expected for the $2''$ beam size of the observations. The outer radius is better constrained, since the emission is very sensitive to the value of R_{out} with a positive power-law index. Figure 7 shows the H_2CO 3–2 line spectrum compared with the spectra derived from models with different radial column densities power-law indices. The spectra suggest a lack of high velocity line wings associated with emission originating in the inner regions of the disk, consistent with the results of the χ^2 analysis.

3.2.2. Ring Model

The positive power-law index found for the H_2CO radial distribution implies that H_2CO is present mainly in the outer disk. This is expected if H_2CO forms *in situ* from CO ice hydrogenation and is therefore present mainly beyond the CO snow-line, previously determined to be at 160 AU by Qi et al. (2011). Guided by this astrochemical *ansatz*, we have tried a second "ring" model where the H_2CO gas is only present where CO has frozen out. The vertical surface boundary is then defined by the CO freeze-out temperature of 19 K (Qi et al. 2011), while the midplane boundary can be constrained by the excitation of multiple H_2CO transitions, as in the power-law model. Within this layer, the abundance of H_2CO is assumed to follow that of H nuclei with a constant fractional abundance, which is also a parameter fit to the data.

The best-fit abundance is 5.5×10^{-11} and the midplane boundary σ_m is consistent with what we find in the power-law model (Table 2). Figure 3 shows that the vertical surface boundary at 19 K effectively results in a ring-like radial structure, where the inner edge of the ring is at CO snow line. Figure 3 also shows that the best-fit power-law and ring models result in similar H_2CO column densities beyond the CO snow line. The profile of the ring model is considerably flatter than the power-law model and even drops outside of 300 AU exponentially to the edge of CO emission. Figures 4–5 show that the power-law model and the ring model channel maps display some subtle differences. But both provide good fits to the data within the noise of the SMA observations. The same model also provides a good match to the N_2H^+ flux, but the combination of low signal-to-noise and observations of just one transition preclude any independent modeling of the N_2H^+ distribution.

3.3. H$_2$CO Excitation Temperatures

HD 163296 is very favorable for H$_2$CO and N$_2$H$^+$ imaging since its relatively high luminosity and massive disk puts the CO snow line at a large angular distance compared to other disks, enabling us to resolve the H$_2$CO and N$_2$H$^+$ emission. Without such spatial information, however, we can still obtain a constraint on where H$_2$CO emission originates in disks based on the average H$_2$CO excitation temperatures. As a gross approximation, H$_2$CO that coexists with CO ice should be cold, i.e. present at an excitation temperature comparable to the CO freeze-out temperature. To test the viability of using excitation temperatures to constrain the H$_2$CO distribution we extracted spectra from three of the HD 163296 simulations presented in §3.2, selecting models with the best outer radius, no inner hole and power-law indices of -2, 0, and 2. These distributions approximately correspond to a H$_2$CO abundance that follows the H$_2$ column, that keeps constant with radius and that increases steeply, forming a ring. Assuming LTE, that both H$_2$CO transitions trace the same underlying populations, and a single rotational excitation temperature, $T_{\rm rot}$, we calculate

$$T_{\rm rot} = \frac{E_1 - E_0}{ln\left((\nu_1 S\mu_1^2 \int T_0 dv)/(\nu_0 S\mu_0^2 \int T_1 dv)\right)}, \tag{1}$$

where E_0 and E_1 are the upper energy levels for the low and high H$_2$CO transitions used in the calculation (H$_2$CO $3_{0,3} - 2_{0,2}$ and $4_{1,4} - 3_{1,3}$ for most disks), ν and $S\mu^2$ the corresponding line frequencies and temperature independent transition strengths and dipole moments, $\int T dv$ the integrated line intensity, which is calculated from the integrated fluxes based on $F/T = 13.6\lambda^2/(a \times b)$, where F is the flux in Jy, T the intensity in K, λ the line wavelength in millimeters, and a and b the emission diameters in $''$. Because of both vertical and radial temperature gradients in the disk, the size dependence of the emission regions from two transitions is complicated but the emission area is not expected to be very different. For simplicity we assume the extent of the emission is the same for both transitions on account

of the model dependent effects of the temperature gradients. All of the line parameters were gathered from Splatalogue (a transition-resolved compilation of several spectroscopic databases), with the data originating from CDMS (Müller et al. 2005). LTE is a reasonable approximation if H_2CO is mainly present at high densities. The critical densities for the observed H_2CO transitions vary between 10^5 and 5×10^6 cm^{-3} (Troscomptet al. 2009), dependent on assumed kinetic temperatures. At radii <300 AU, all gas colder than 25 K is at densities higher than 10^7 cm^{-3} (Qi et al. 2011), justifying this assumption.

Using the simulated spectra we derive an excitation temperature of 27 K for the model with $p = -2$ and excitation temperatures close to or below 20 K for the other two models. Excitation temperatures thus provide some constraints on the H_2CO distribution, but a temperature close to the expected CO freeze-out temperature only implies an increasing abundance with radius; it cannot be used to assess how steeply the abundance increases.

By combining the new H_2CO detections toward TW Hya and HD 163296 with H_2CO data from DISCS (Öberg et al. 2010, 2011b), we have a sample of 10 disks with two H_2CO line detections or one H_2CO line detection and one upper limit (Table 3). These data are sufficient to calculate excitation temperatures, albeit with substantial uncertainties. Figure 8 shows the calculated excitation temperatures for 9 of the 10 disks; the chemically peculiar Herbig Ae star HD 142527 is not included because its excitation temperature of 250 K is probably not due to thermal excitation.

The H_2CO excitation temperature, listed in Table 3, is consistent with, or lower than, the CO freeze-out temperature of $\sim$20 K for all of these disks. The average H_2CO temperature in the sample (excluding HD 142527) is 18 ± 6 K. We note that the relatively high excitation temperature toward HD 163296 is most likely due to the fact that some H_2CO 3–2 emission is resolved out by the SMA observations, as the compact-north antenna configuration has few short baselines.

3.4. H_2CO/N_2H^+ Correlations

We examine the disk sources to test if N_2H^+ and H_2CO emission are correlated across the sample, as would be expected if 1) the two molecules form under the same physio-chemical conditions, i.e. only in the regions where CO has frozen out, 2) the line emission trace the total N_2H^+ and H_2CO column well, and 3) midplane ionization levels and CO hydrogenation efficiencies do not differ 'too much' across the sample (i.e. the size of the CO freeze-out region is the most important regulator of N_2H^+ and H_2CO column across the sample). It should be noted that there are other scenarios that could produce a correlation as well, and that the correlation analysis below should only be considered as a constraint on the H_2CO distribution in combination with the results in the previous sections. In particular a constant H_2CO/N_2H^+ across a disk sample would be expected if the relative fractions of chemically characteristic disk regions is always similar in disks. To conclusively test this requires a larger sample than currently available, but the fact that we did not find that H_2CO emission correlates with any other molecular emission than N_2H^+ already challenges this scenario.

Where possible, we base the comparison on the H_2CO $3_{0,3} - 2_{0,2}$ line that has $E_{up} = 21$ K, similar to N_2H^+ $J = 3 - 2$ ($E_{up} = 27$ K), to minimize variations in fluxes caused by the different detailed temperature structures in different disks. Excluding HD 142527, this line has been observed toward 6/9 of the sample. For the remaining 3/9 disks, we calculate the expected H_2CO $3_{0,3} - 2_{0,2}$ line flux based on the H_2CO excitation temperatures and fluxes of other H_2CO lines toward each source. We then normalize the flux of each H_2CO $3_{0,3} - 2_{0,2}$ line to the (Taurus) distance of 140 pc, and we further normalize to a disk mass of 0.01 $M_\odot$ to account for the fact that more nearby and more massive disks tend to have overall stronger line emission. Figure 9 shows that there is a strong correlation between the normalized H_2CO and N_2H^+ fluxes in the disk sample; the

rank correlation is statistically significant at the 95% level. As expected, Figure 10 shows that this implies a nearly constant N_2H^+ 3-2 / H_2CO $3_{0,3} - 2_{0,2}$ flux ratio across the sample.

4. Discussion

Our modeling strategy in this study and in Qi et al. (2008) has been to first constrain the overall structure of molecular emission in disks using a parametric model with a minimum of free parameters, i.e. to determine whether the radial column density profile of a species decreases, increases or is flat as a function of disk radius. As demonstrated in Öberg et al. (2012), the slope of the radial column density profile already can place significant constraints on the formation pathway of a molecule. Here we find that H_2CO toward HD 163296 belongs to the family of molecules that display an increasing column density with radius. This first-order constraint on the H_2CO distribution motivated us to consider H_2CO formation pathways that would result in an increase of H_2CO with disk radius. H_2CO formation through CO-ice hydrogenation results in a simple prediction that H_2CO should be present in a ring, with the inner edge at the CO snow line. We therefore set up a second model, based on this prediction, to test if the observations are consistent with this hypothesis for H_2CO formation. We propose that this combination of backward and forward modeling both provides a fair view of the constraints obtained by fitting the data, and challenges our basic understanding of disk chemistry.

4.1. H_2CO Formation

H_2CO can form through multiple chemical pathways. We have shown that the H_2CO distribution towards HD 163296 and the sample statistics are consistent with formation through *in situ* CO ice hydrogenation. Here we consider the effects of additional pathways

for H_2CO formation, in particular (1) *in situ* gas phase formation, and (2) formation in the pre- and proto-stellar phases, followed by incorporation into the disk.

H_2CO can form in the gas-phase through ion-neutral reactions involving, e.g. CH_3^+ or through neutral-neutral reactions between CH_3 and O (e.g. Aikawa & Herbst 1999). The neutral-neutral formation pathway is expected to result in a radially flat column density structure for a typical T Tauri disk (Aikawa & Herbst 1999), with most emission originating at temperatures of 20-40 K (Aikawa et al. 2003). It is not clear from existing disk models whether the structure will look substantially different if the neutral-ion reactions dominate. In a protostellar chemistry model (Bergin & Langer 1997), CH_3^+ disappears when CO depletes (E. Bergin, private communication). This suggests that H_2CO forming through this pathway should be anti-correlated with CO-freeze-out. Neither of these gas-phase pathways thus predicts excess H_2CO column densities in the outer disk, or at low (T<20 K) temperatures. The observed low excitation temperature could on its own be explained by efficient turbulent mixing of H_2CO formed in the gas-phase and then cooled down in the midplane regions, similarly to what has been proposed to explain cold CO gas in disks (Aikawa 2007). Turbulent mixing would not, however, explain the observed deficiency of H_2CO towards the inner disk in HD 163296. Gas-phase formation of H_2CO then seems an unlikely dominant source of H_2CO in disks in light of the new observations, but the case is unlikely to be conclusively settled until the exclusive grain-surface product CH_3OH is observed to display a similar distribution.

H_2CO in disks could be a product of protostellar or molecular cloud chemistry, as H_2CO is commonly observed in pre- and protostellar sources, and this molecular content may be preserved, at least in part, through the process of disk formation. Willacy (2007) has modeled this scenario, starting with a H_2CO ice abundance of $10^{-6}n_H$ inherited from the cold cloud. The model also includes H_2CO formation through gas-phase processes

in the disk and results are presented with and without photodesorption. In the model without photodesorption, H_2CO follows CO in the inner disk and has an additional outer disk component with an abundance that decreases with radius beyond the CO snow line. When photodesorption is included, the H_2CO column is flat across the disk, corresponding to a power-law index of 0. Neither predicted abundance pattern is consistent with the new observations. In addition, H_2CO is common towards protostellar sources of a range of luminosities (e.g. Schöier et al. 2004; Bisschop et al. 2007), while it is pre-dominantly detected towards disks around the low luminosity T Tauri stars.

In short, H_2CO formation through *in situ* CO-ice hydrogenation is not only consistent with the observations, but it is the *only* pathway proposed (so far) that naturally explains the observations. To conclusively demonstrate a CO-ice hydrogenation origin would, however, require the detection of co-spatial emission of CH_3OH; CH_3OH has no known efficient gas-phase formation pathway and is predicted to form together with H_2CO whenever CO ice is hydrogenated (Cuppen et al. 2009).

4.2. Locating the CO "Snow Line"

The "snow line" is typically used to denote the midplane disk radius at which the temperature is low enough for water to condense out on dust grains. Outside of the snow line, grain accretion will be faster because of larger and stickier grains, which may substantially speed up the formation of planetesimals and eventually planets (e.g. Hayashi 1981; Ida & Lin 2004, 2008; Ciesla & Cuzzi 2006; Kretke & Lin 2007). In the Solar System, the dividing line between rocky planets and gas giants coincide with the H_2O snow line (Lewis 1974). CO is another abundant volatile in disks and its snow line may boost planet formation in the outer disk by providing extra solid masses (Dodson-Robinson et al. 2009) and inducing planet traps (Masset et al. 2006; Hasegawa & Pudritz 2012), and could affect

the elemental make-up of the forming gas-giants (Öberg et al. 2011a). Because of its high volatility ($T_{\text{freeze-out}} \sim 20$ K), the CO snow line is expected at disk radii of 10s–100s of AU. This should make it a far more accessible target than the H_2O snow line for millimeter interferometry studies aimed at examining the general effects of snow lines on disk structures.

Localizing the CO snow line directly from millimeter CO data is challenging, however. Disks have both a radial temperature gradient away from the central star, and a vertical one set by radiative heating at the disk surface (e.g. Aikawa & Herbst 1999). This results in a CO condensation front that is located at different radii at different disk heights (Fig. 11), and also that some CO is present at all radii in the upper disk layers. This fact, together with a complex radiative transfer (most CO lines are expected to be optically thick in the disk center and optically thin in the outer parts of the disk), means that the location of a CO snow line in a disk cannot be inferred from simply inspecting a CO disk image. The best constraint that exists to date on a CO snow line radius is toward the Herbig Ae star HD 163296 based on the analysis of multi-transition, multi-isotope, spatially resolved CO line data on a self-consistent physical disk model (Qi et al. 2011). The temperature structure of the model has been constrained by optically thick multiple CO lines and detailed analysis of the optically thinner ^{13}CO emission reveals a significant column density reduction at around 165 AU that cannot be explained by the overall disk column distribution as traced by the dust. This is interpreted as the result of CO freeze-out and the location as the CO snow line. Uncertainties in the temperature structure will mainly affect the determination of the CO freeze-out temperature at the location of the CO snow line, rather than the location itself , which is constrained between 135 and 175 AU in the disk of HD 163296. While fruitful, this is a time consuming approach that will be difficult to apply to larger samples of disks and will always include some degree of model dependency.

Another approach to constrain the CO snow line location is to identify trace species that are only present where CO has begun to freeze out. Such molecules should display a ring-like structure with the inner edge corresponding to the midplane CO snow line. As we have described, N_2H^+ and H_2CO are good candidate probes of CO snow lines. In principle, these species can be used as powerful chemical imaging tools to constrain CO snow line locations in large samples of disks, rather than relying on complex analysis of the CO isotopologue observations.

4.2.1. Simulated ALMA Observations

It seems clear that both N_2H^+ and H_2CO are outer-disk species from the chemical perspective. To connect their formation to the onset of CO freeze-out conclusively requires a combination of higher sensitivity, and higher resolution imaging. This kind of imaging can be done with the newly available capabilities of the ALMA telescope in Chile, which is nearing completion of construction.

To demonstrate the astrochemical predictions generated by our analysis of the SMA data, and the ease at which they can be tested with ALMA, we present a set of simulations of HD 163296 ALMA observations using the antenna configuration 5 (corresponding to $0.3''$ resolution) in Figure 12. The predicted H_2CO and N_2H^+ rings are readily detected at this resolution, and the power-law and ring models are clearly distinguished. For both models, the diameter of the emission maximum can be estimated directly from the images within a fraction of the beam size, enabling us to determine if the H_2CO and N_2H^+ emission truly trace the CO snow line. In addition, ALMA should have sufficient sensitivity to detect CH_3OH if it is present with a similar abundance and distribution as H_2CO, as expected if both of these species are formed through CO hydrogenation and then non-thermally desorbed.

5. Conclusions

We have presented three observational results that support the idea that CO freeze-out regulates the H_2CO and N_2H^+ chemistry in disks:

1. H_2CO and N_2H^+ emission towards HD 163296 appears offset from the continuum peak at a size scale consistent with the CO snow line at 160 AU. These observations are matched well by a ring model where H_2CO is present only in the disk regions with CO freeze-out.

2. The H_2CO excitation temperature in a sample of 9 disks is typically below ~ 20 K, consistent with the bulk of H_2CO emission originating in disk regions where CO is expected to freeze-out.

3. The H_2CO and N_2H^+ emission are correlated across the disk sample, consistent with the hypothesis of coexistence beyond the CO snow line.

These results suggest that both N_2H^+ and H_2CO should be present in rings, with the inner edge at the CO snow line. This may be used as a probe of CO snow line locations across samples of disk and is also important for predicting the organic content of comets forming at different disk radii. In general, the radial and vertical distributions of molecules constitute strong probes of the basic chemistry used into astrochemical models, while molecular abundances and column densities are probably best used to test our understanding of the structure and history of individual objects.

Facilities: SMA

REFERENCES

Aikawa, Y. & Herbst, E. 1999, A&A, 351, 233

Aikawa, Y., Momose, M., Thi, W., et al. 2003, PASJ, 55, 11

Aikawa, Y. & Nomura, H. 2006, ApJ, 642, 1152

Aikawa, Y. 2007, ApJ, 656, L93

Aikawa, Y., van Zadelhoff, G. J., van Dishoeck, E. F., & Herbst, E. 2002, A&A, 386, 622

Andrews, S., Wilner, D., Espaillat, C., et al. 2011, ArXiv e-prints

Andrews, S. M. & Williams, J. P. 2005, ApJ, 631, 1134

Andrews, S. M., Wilner, D. J., Hughes, A. M., Qi, C., & Dullemond, C. P. 2009, ApJ, 700, 1502

Bergin, E. A. & Langer, W. D. 1997, ApJ, 486, 316

Bergin, E. A., Alves, J., Huard, T., & Lada, C. J. 2002, ApJ, 570, L101

Bisschop, S. E., Jørgensen, J. K., van Dishoeck, E. F., & de Wachter, E. B. M. 2007, A&A, 465, 913

Caselli, P., Walmsley, C. M., Tafalla, M., Dore, L., & Myers, P. C. 1999, ApJ, 523, L165

Ciesla, F. J. & Cuzzi, J. N. 2006, Icarus, 181, 178

Cuppen, H. M., van Dishoeck, E. F., Herbst, E., & Tielens, A. G. G. M. 2009, A&A, 508, 275

Dodson-Robinson, S. E., Willacy, K., Bodenheimer, P., Turner, N. J., & Beichman, C. A. 2009, Icarus, 200, 672

Dutrey, A., Guilloteau, S., & Guelin, M. 1997, A&A, 317, L55

Dutrey, A., Henning, T., Guilloteau, S., et al. 2007, A&A, 464, 615

Fuchs, G. W., Cuppen, H. M., Ioppolo, S., et al. 2009, A&A, 505, 629

Garrod, R. T., Wakelam, V., & Herbst, E. 2007, A&A, 467, 1103

Hasegawa, Y. & Pudritz, R. E. 2012, ArXiv e-prints

Hayashi, C. 1981, in IAU Symposium, Vol. 93, Fundamental Problems in the Theory of
    Stellar Evolution, ed. D. Sugimoto, D. Q. Lamb, & D. N. Schramm, 113–126

Henning, T. & Semenov, D. 2008, in IAU Symposium, Vol. 251, IAU Symposium, ed.
    S. Kwok & S. Sandford, 89–98

Hogerheijde, M. R. & van der Tak, F. F. S. 2000, A&A, 362, 697

Ida, S. & Lin, D. N. C. 2004, ApJ, 616, 567

Ida, S. & Lin, D. N. C. 2008, ApJ, 685, 584

Jørgensen, J. K. 2004, A&A, 424, 589

Kretke, K. A. & Lin, D. N. C. 2007, ApJ, 664, L55

Lewis, J. S. 1974, Science, 186, 440

Lombardi, M., Lada, C. J., & Alves, J. 2008, A&A, 489, 143

Masset, F. S., Morbidelli, A., Crida, A., & Ferreira, J. 2006, ApJ, 642, 478

Müller, H. S. P., Schlöder, F., Stutzki, J., & Winnewisser, G. 2005, Journal of Molecular
    Structure, 742, 215

Mumma, M. J. & Charnley, S. B. 2011, ARA&A, 49, 471

Öberg, K. I., Linnartz, H., Visser, R., & van Dishoeck, E. F. 2009a, ApJ, 693, 1209

Öberg, K. I., Murray-Clay, R., & Bergin, E. A. 2011a, ApJ, 743, L16

Öberg, K. I., Qi, C., Fogel, J. K. J., et al. 2010, ApJ, 720, 480

Öberg, K. I., Qi, C., Fogel, J. K. J., et al. 2011b, ApJ, 734, 98

Öberg, K. I., Qi, C., Wilner, D. J., & Andrews, S. M. 2011c, ApJ, 743, 152

Öberg, K. I., Qi, C., Wilner, D. J., & Hogerheijde, M. R. 2012, ApJ, 749, 162

Öberg, K. I., van Broekhuizen, F., Fraser, H. J., et al. 2005, ApJ, 621, L33

Öberg, K. I., van Dishoeck, E. F., & Linnartz, H. 2009b, A&A, 496, 281

Pinte, C., Padgett, D. L., Ménard, F., et al. 2008, A&A, 489, 633

Qi, C., D'Alessio, P., Öberg, K. I., et al. 2011, ApJ, 740, 84

Qi, C., Ho, P. T. P., Wilner, D. J., et al. 2004, ApJ, 616, L11

Qi, C., Kessler, J. E., Koerner, D. W., Sargent, A. I., & Blake, G. A. 2003, ApJ, 597, 986

Qi, C., Wilner, D. J., Aikawa, Y., Blake, G. A., & Hogerheijde, M. R. 2008, ApJ, 681, 1396

Qi, C., Wilner, D. J., Calvet, N., et al. 2006, ApJ, 636, L157

Rodriguez, D. R., Kastner, J. H., Wilner, D., & Qi, C. 2010, ApJ, 720, 1684

Schöier, F. L., Jørgensen, J. K., van Dishoeck, E. F., & Blake, G. A. 2004, A&A, 418, 185

Schöier, F. L., van der Tak, F. F. S., van Dishoeck, E. F., & Black, J. H. 2005, A&A, 432, 369

Thi, W., van Zadelhoff, G., & van Dishoeck, E. F. 2004, A&A, 425, 955

Tielens, A. G. G. M. & Hagen, W. 1982, A&A, 114, 245

Troscompt, N. and Faure, A. and Wiesenfeld, L. and Ceccarelli, C. and Valiron, P. 2009, A&A, 493, 687

Verhoeff, A. P., Min, M., Pantin, E., et al. 2011, A&A, 528, A91

Walsh, C., Nomura, H., Millar, T. J., & Aikawa, Y. 2012, ApJ, 747, 114

Watanabe, N., Shiraki, T., & Kouchi, A. 2003, ApJ, 588, L121
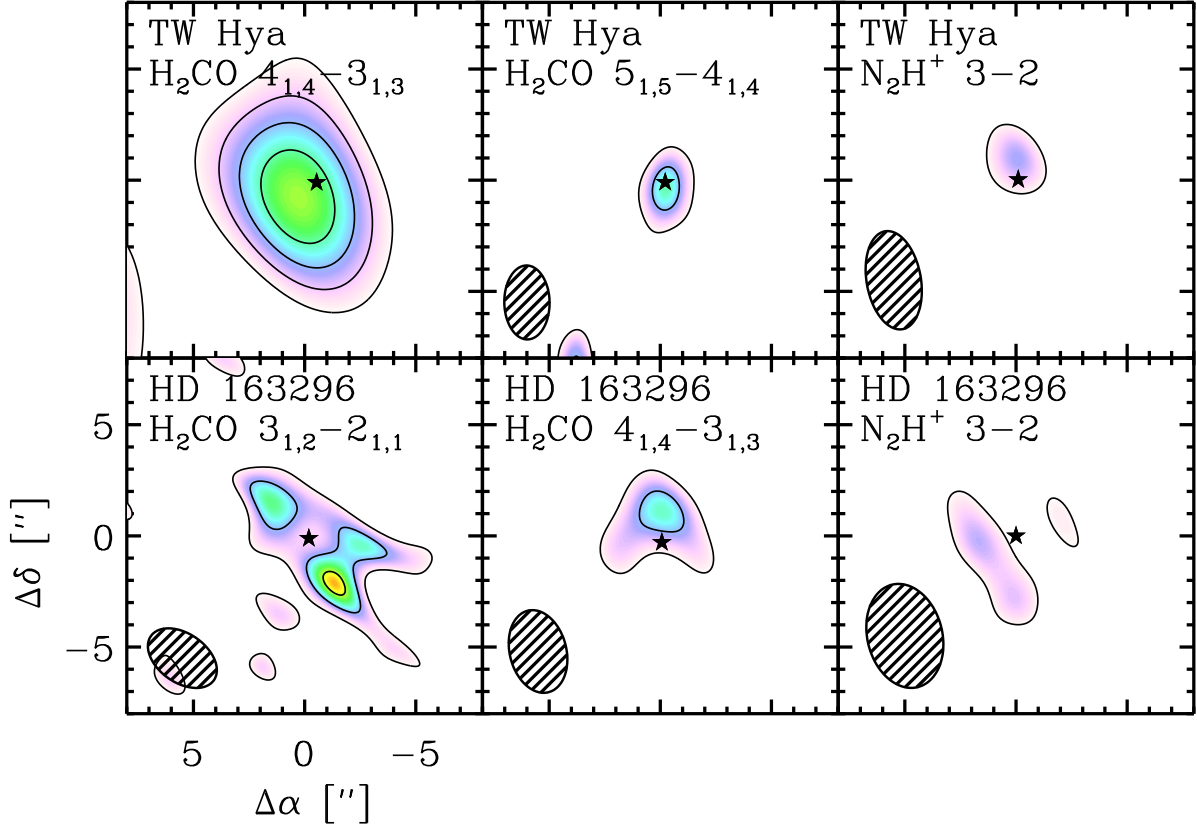
Willacy, K. 2007, ApJ, 660, 441

Fig. 1.— H_2CO and N_2H^+ observations toward TW Hya and HD 163296 with the SMA. The emission toward TW Hya is centrally peaked, while there is a clear offset in the H_2CO emission toward HD 163296. The first two contour levels are 3 and 5σ, with 1σ measured to be 0.10 (H_2CO 4–3), 0.13 (H_2CO 5–4), and 0.36 (N_2H^+) Jy km s^{-1} per beam toward TW Hya, and 0.06 (H_2CO 3–2), 0.17 (H_2CO 4–3), and 0.13 (N_2H^+) Jy km s^{-1} per beam toward HD 163296.
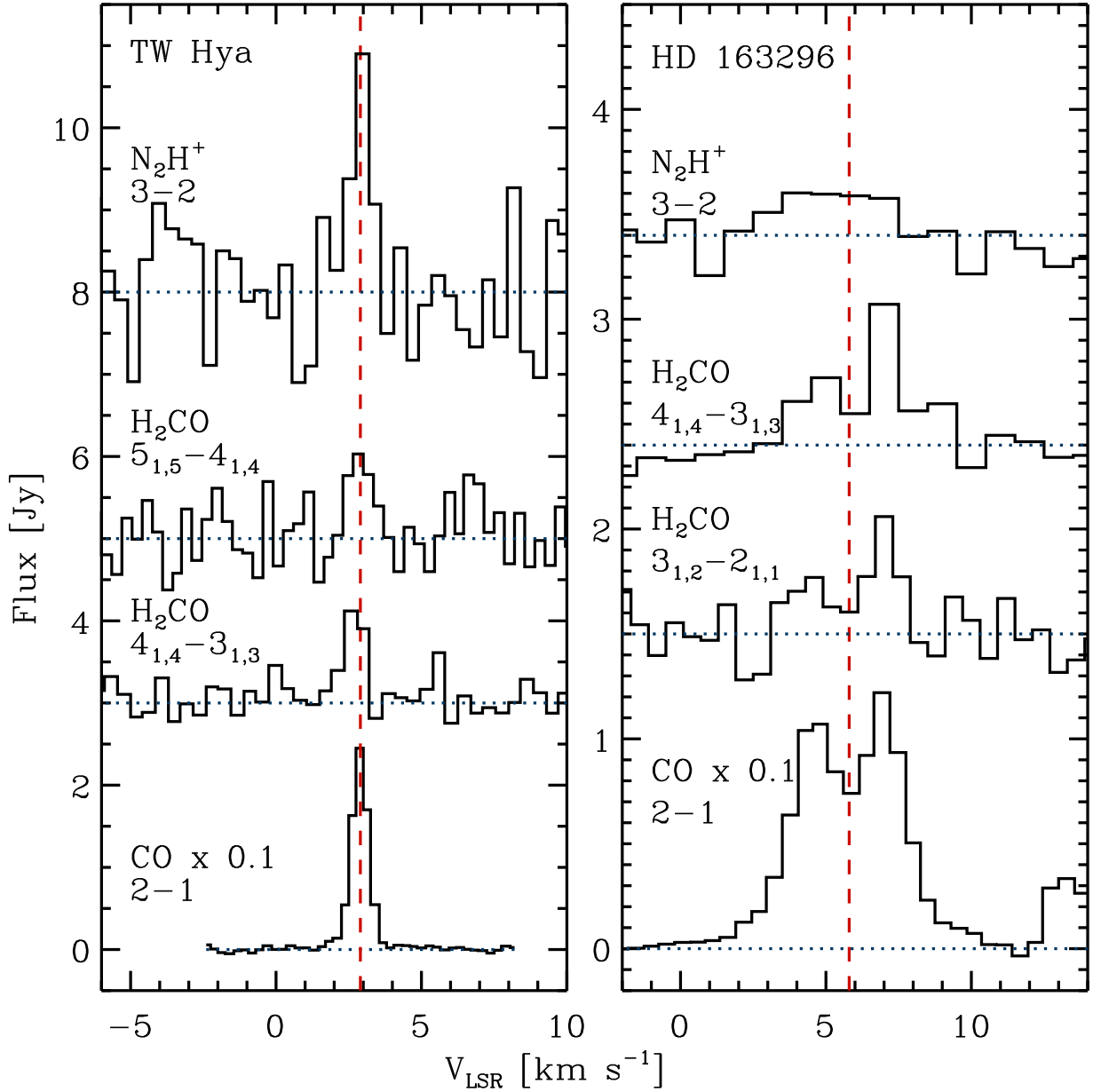
Fig. 2.— Spatially integrated spectra of H_2CO and N_2H^+ toward TW Hya and HD 163296. The red dashed lines mark V_{LSR} toward each source, based on CO observations (Qi et al. 2006, 2011). The double-peak structure typical for rotating disks is not resolved toward TW Hya with the applied spectral resolution because of its face-on orientation.
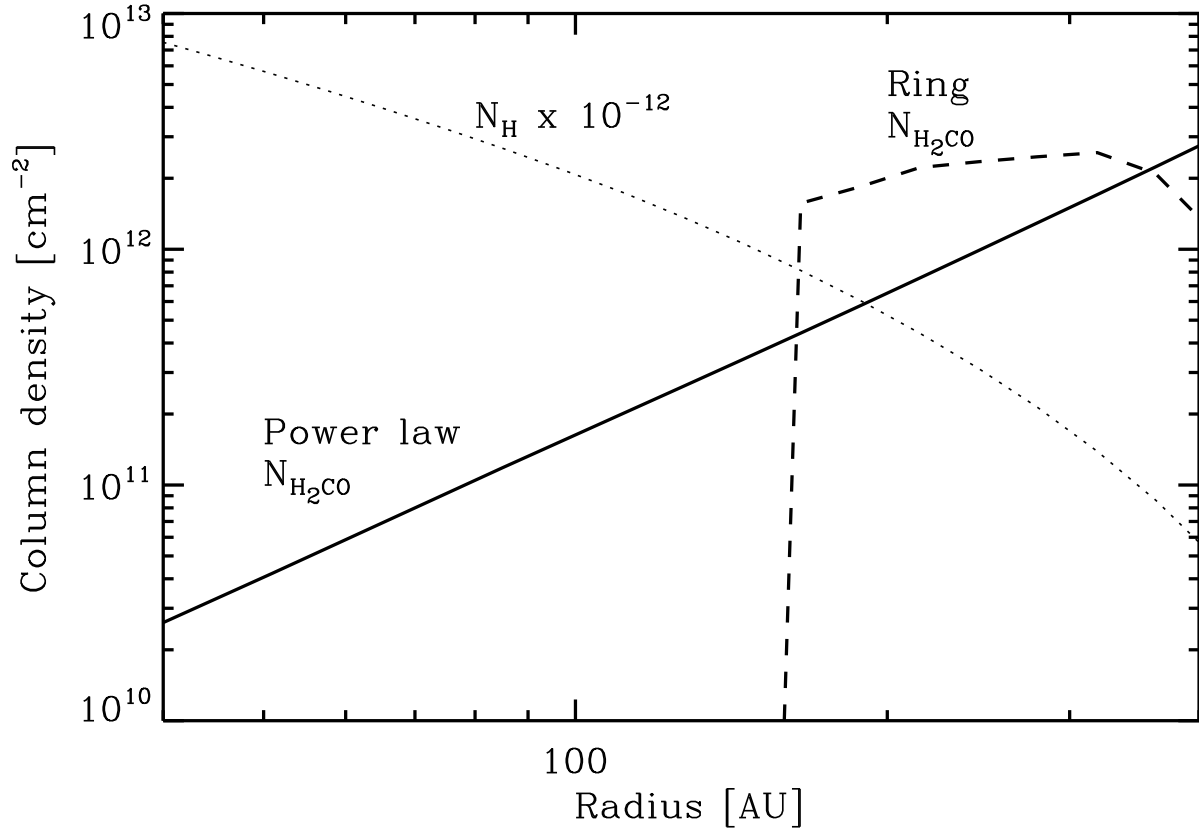
Fig. 3.— The hydrogen nuclei column density toward HD 163296 (Qi et al. 2011) is plotted together with the H_2CO column density from the best-fit power law and 'ring' models. In the ring model, the H_2CO abundance is defined to be zero when the temperature is less than 19 K, the CO freeze-out temperature, which leads to the sharp drop in the H_2CO column density interior to the CO snow line at 160 AU.
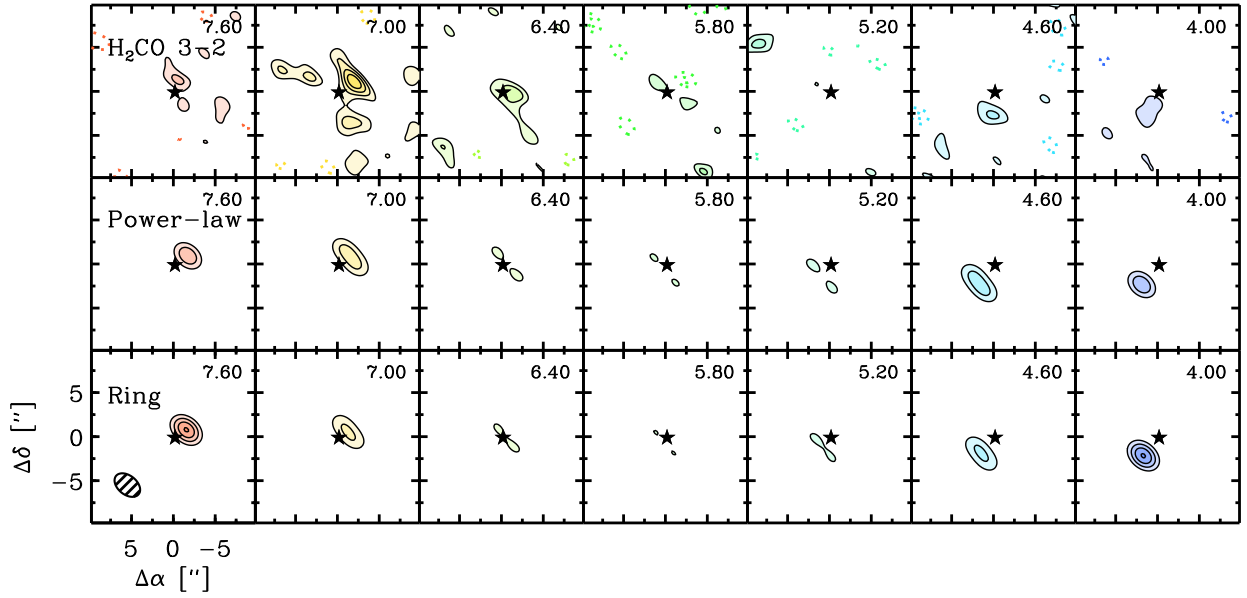
Fig. 4.— Observed and simulated channel maps for H_2CO $3_{1,2} - 2_{1,1}$ toward HD 163296, using the best-fit power-law (p=2) and ring model. Both models fit the data within the uncertainties. The first contour is 2σ and each following contour step is 1σ. The channel velocity in km s^{-1} is in the upper right corner of each panel and the synthesized beam is displayed in the lower left panel.
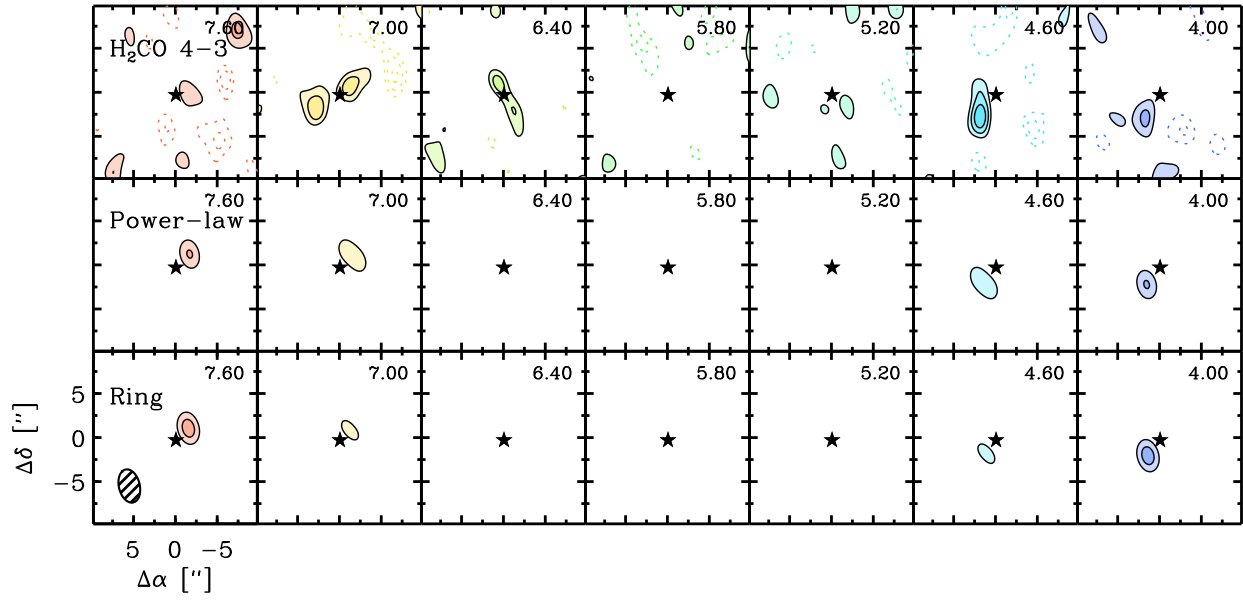
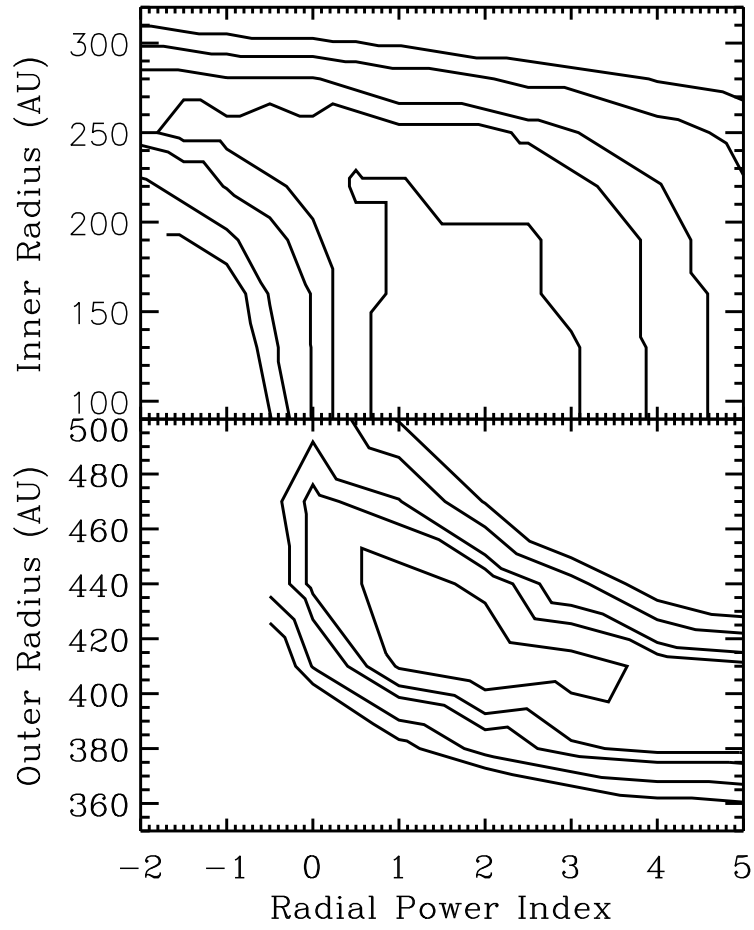Fig. 5.— As Fig. 4 but for the H_2CO $4_{1,4} - 3_{1,3}$ line.

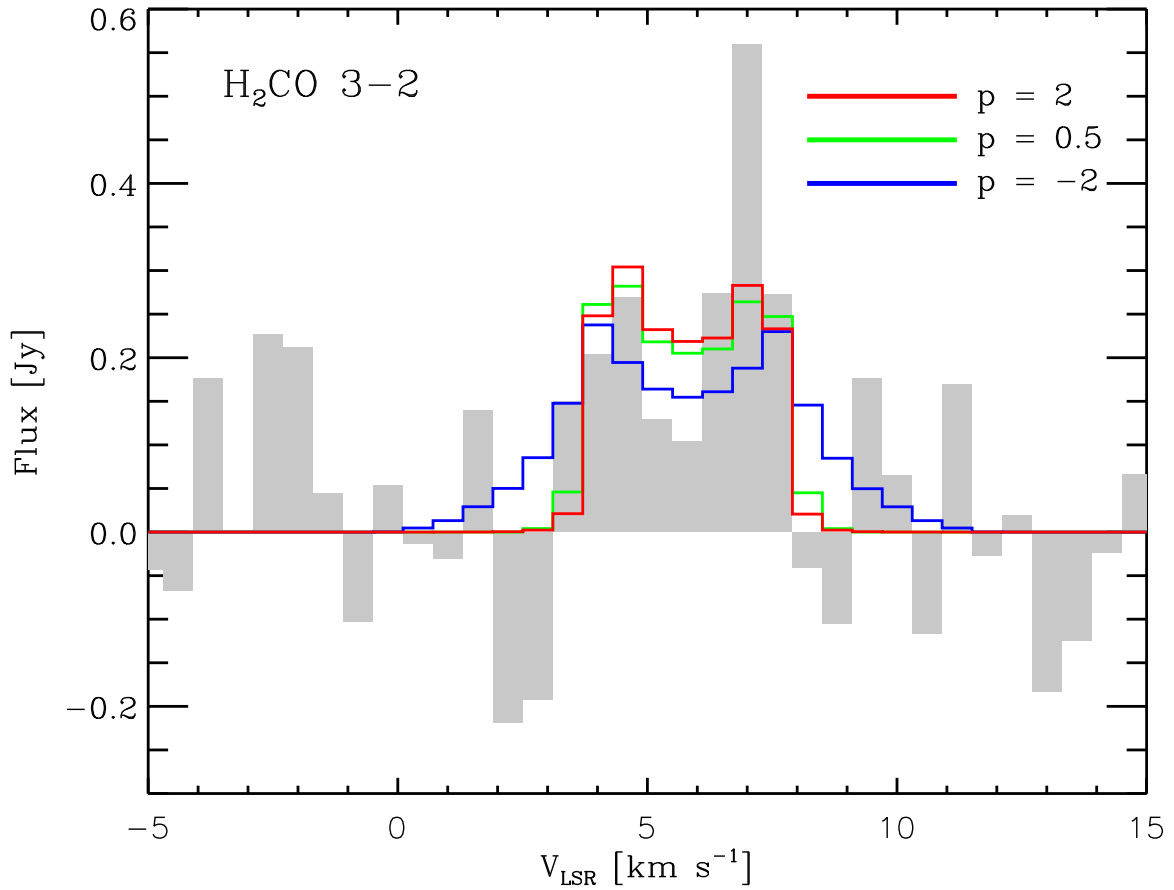Fig. 6.— Iso-χ^2 surfaces of R_{out} and R_{in} versus p. Contours correspond to the 1–5 σ errors.

Fig. 7.— Simulated spectra for H_2CO $3_{1,2} - 2_{1,1}$ for models with radial column densities power-law indices $p = 2$(best-fit, red line), 0.5(within 1σ noise level, green line) and -2(blue line), overlaid with the HD 163296 spectra in gray shade.
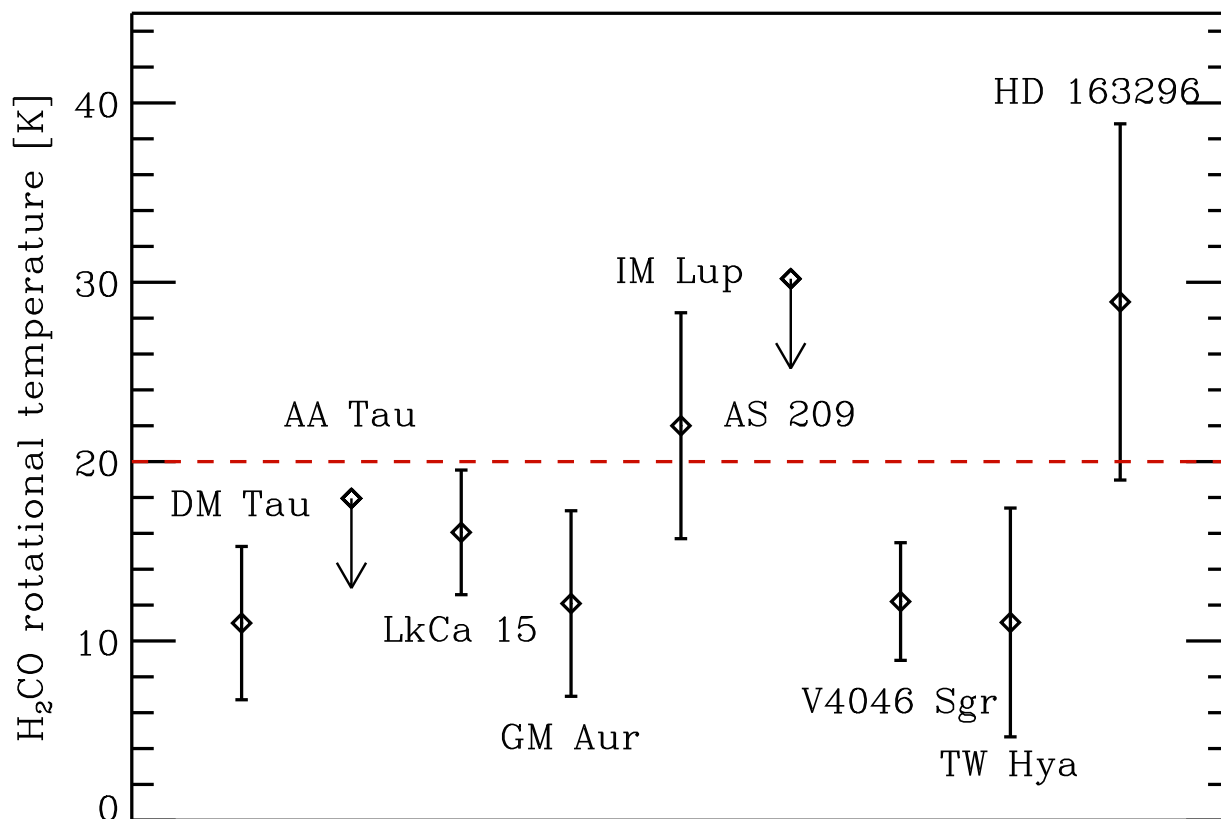
Fig. 8.— The calculated H_2CO excitation temperatures for all disks observed with the SMA that have at least one H_2CO detection and one upper limit, except for the disk around HD 142527, which has a very high excitation temperature of >100 K. All remaining disks have excitation temperatures H_2CO consistent with or lower than the expected CO freeze-out temperature of ~20 K (red dashed horizontal line).
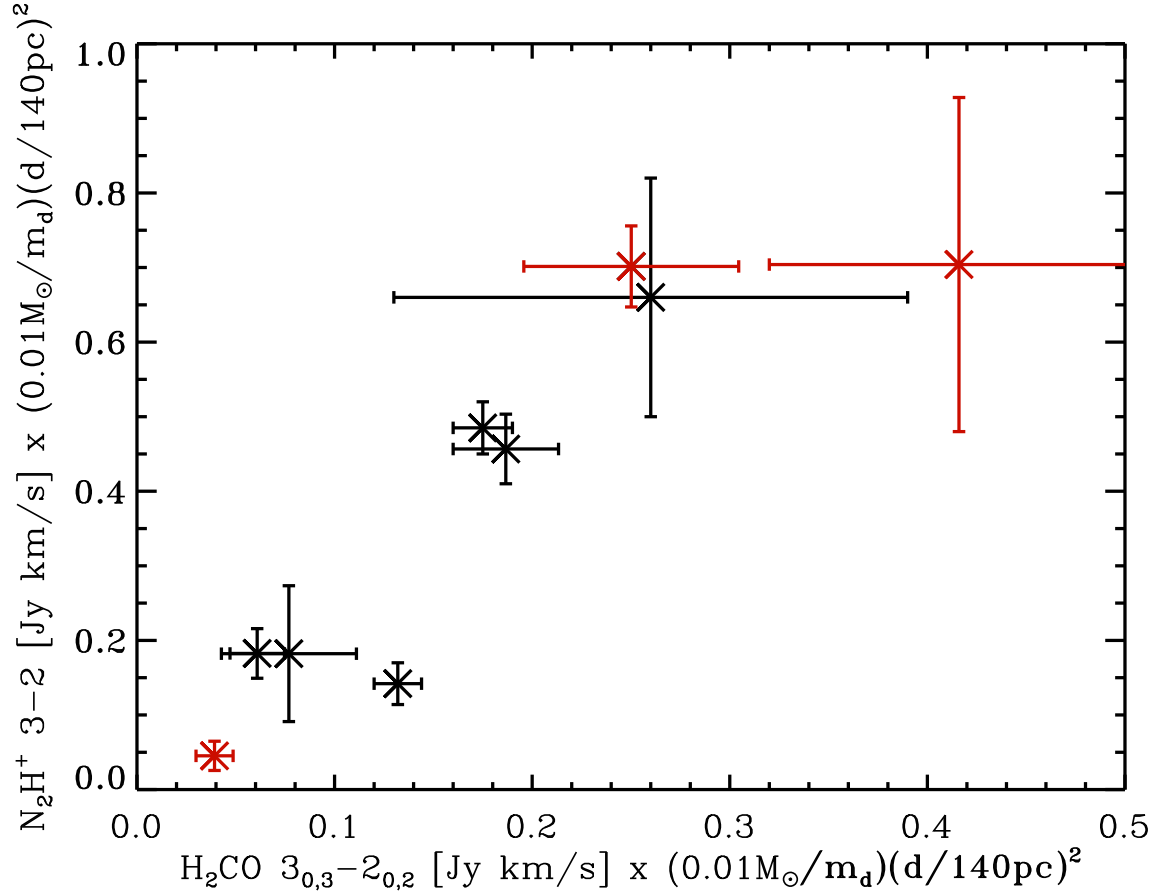
Fig. 9.— Correlation of N_2H^+ 3–2 ($E_u = 27$ K) and H_2CO $3_{0,3} - 2_{0,2}$ ($E_u = 21$ K) emission normalized to disk mass (based on dust modeling) and source distance. The red symbols mark disks where the H_2CO $3_{0,3} - 2_{0,2}$ flux has been calculated based on the flux from other H_2CO transitions.
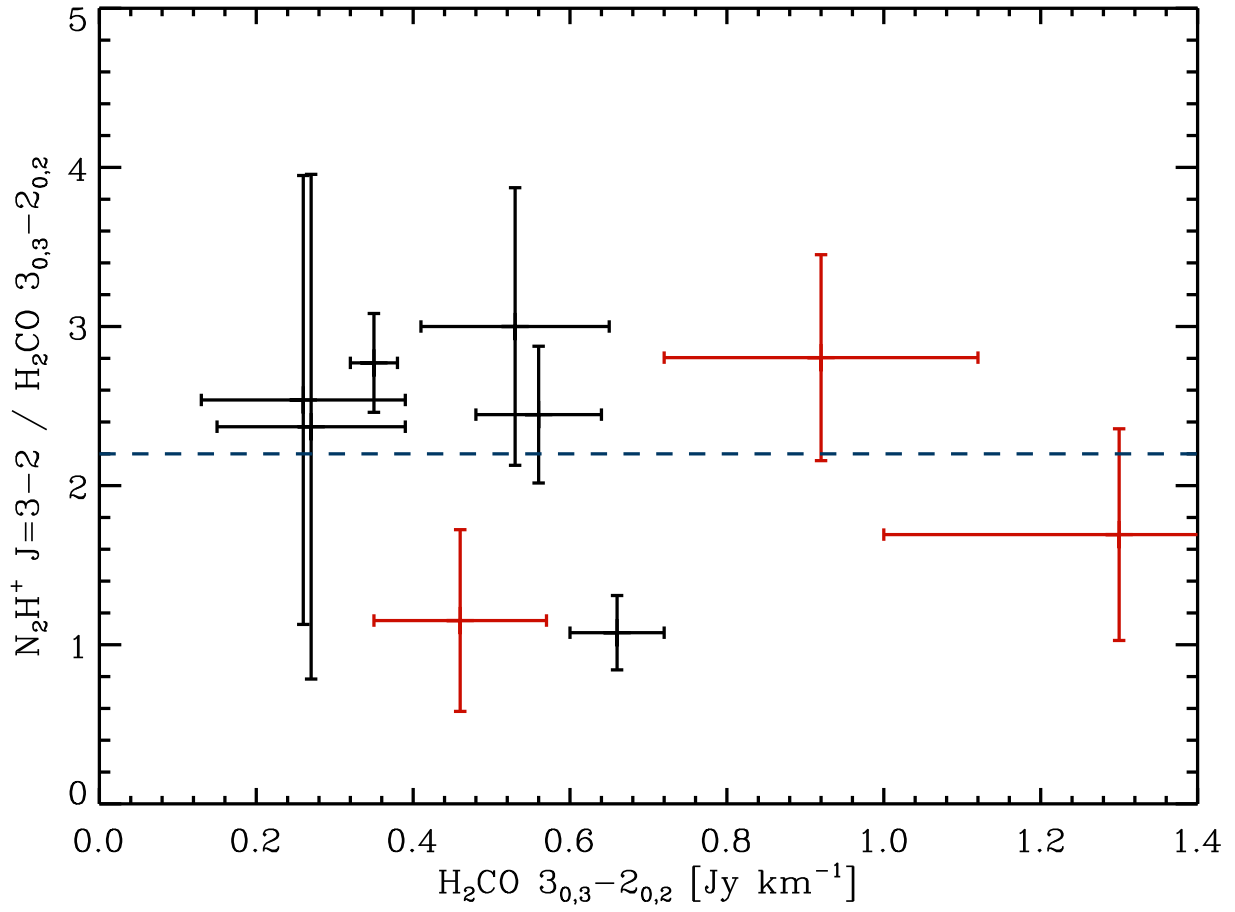
Fig. 10.— The N_2H^+/H_2CO ratio, demonstrating that it is almost constant, as would be expected from the strong correlation between the normalized fluxes.

Fig. 11.— Illustration of the expected distribution of CO in the gas-phase and on grain-surfaces. Co freeze-out beyond the CO-snow line (R_{20K}) and interior to the dashed contour is predicted to result in a large increase of N_2H^+ and the onset of H_2CO production from CO ice. The ice may then non-thermally desorb to produce gas-phase H_2CO.

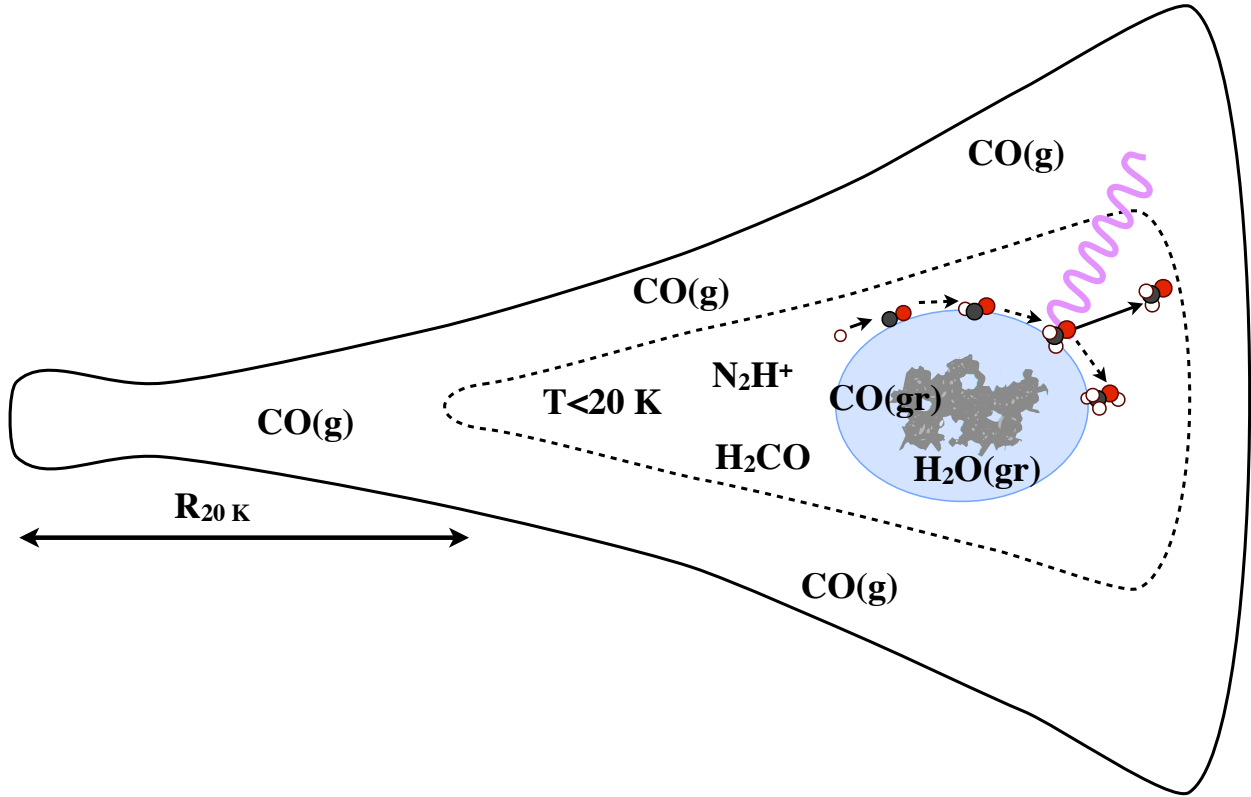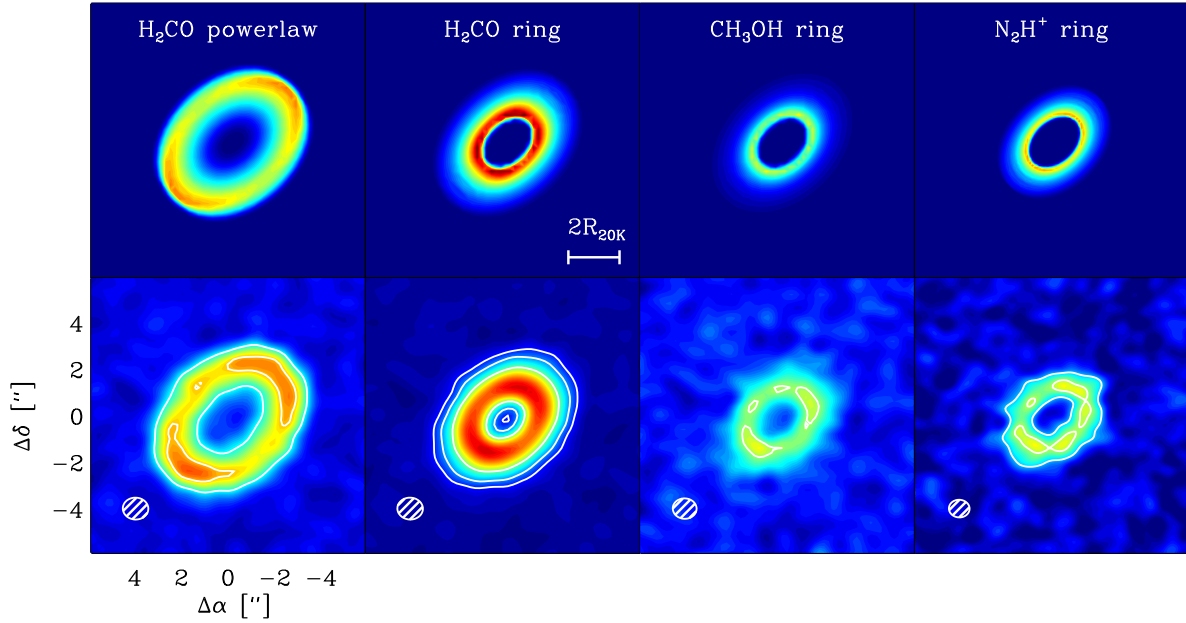Fig. 12.— The predicted morphology of H$_2$CO 3–2 emission toward HD 163296 for the power-law and ring model, when using ALMA antenna configuration 5 (corresponding to 0.3$''$ resolution) and 1h integration. The H$_2$CO ring structure should be accompanied by similar CH$_3$OH and N$_2$H$^+$ rings if the observations reported in this paper are due the exclusive presence of H$_2$CO in the outer disk, exterior to the CO snow line. For the CH$_3$OH simulation we assumed the same column density and excitation temperature for CH$_3$OH as has been observed for H$_2$CO, and imaged the 241.767 GHz $5_{0,5} - 4_{0,4}$ line. White contours are [0.025,0.05,0.1] Jy km s^{-1} per beam.

Table 1: Observational Parameters[a]

Parameter	HD 163296		
	2007 Mar 20 (COM-N)	2012 Jun 10 (COM)	2012 Jun 10 (COM)
			2012 Aug 12 (SUB)
			2012 Aug 14 (SUB)
Baseline (m)	16.4–139.2	16.4–77.0	9.5–77.0
Lines	H_2CO $3_{1,2}$–$2_{1,1}$	H_2CO $4_{1,4}$–$3_{1,3}$	N_2H^+ 3–2
Rest frequency (GHz)	225.69778	281.52693	279.51170
Beam Size (FWHM)	$3''\!.4\times2''\!.2$	$3''\!.9\times2''\!.5$	$4''\!.9\times3''\!.4$
P.A.	54°	15°	14°
Channel spacing ($km\,s^{-1}$)	0.54	0.87	0.60
RMS Noise ($Jy\,beam^{-1}$)	0.063	0.096	0.072
Integrated Flux ($Jy\,km\,s^{-1}$)	0.89	1.55	0.53
Continuum (GHz)	221	273	273
Beam Size (FWHM)	$3''\!.5\times2''\!.2$	$4''\!.1\times2''\!.6$	$5''\!.2\times3''\!.5$
P.A.	56°	15°	14°
RMS Noise ($mJy\,beam^{-1}$)	3.4	9.4	3.8
Flux Density ($Jy\,beam^{-1}$)	0.49	0.96	0.95
Integrated Flux (Jy)	0.61	1.06	1.07
Parameter	TW Hya		
	2012 Jan 13(SUB)	2008 Feb 23 (COM)	2012 Jun 4 (COM)
Baseline (m)	9.5–45.2	16.4–77.0	16.4–77.0
Lines	H_2CO $4_{1,4}$–$3_{1,3}$	H_2CO $5_{1,5}$–$4_{1,4}$	N_2H^+ 3–2
Rest frequency (GHz)	281.52693	351.76866	279.51170
Beam Size (FWHM)	$9''\!.1\times5''\!.6$	$3''\!.3\times2''\!.0$	$3''\!.5\times2''\!.0$
P.A.	24°	1°	10°
Channel spacing ($km\,s^{-1}$)	0.43	0.17	0.11
RMS Noise ($Jy\,beam^{-1}$)	0.16	0.23	0.55
Integrated Flux ($Jy\,km\,s^{-1}$)	1.22	0.54	2.2
Continuum (GHz)	273	346	273
Beam Size (FWHM)	$9''\!.2\times5''\!.7$	$3''\!.5\times2''\!.0$	$4''\!.8\times2''\!.4$
P.A.	25°	-2°	10°
RMS Noise ($mJy\,beam^{-1}$)	6.2	12	14
Flux Density ($Jy\,beam^{-1}$)	0.90	1.20	0.70
Integrated Flux (Jy)	0.93	1.52	0.92

[a]All quoted values assume natural weighting.

Table 2: Best-Fit Model Parameters[a]

Parameter	HD 163296
Power-law Model	
N_{100} (cm^{-2})	1.7×10^{11}
p	2
R_{out} (AU)	410
R_{in} (AU)	<200
Surface boundary σ_s	$10^{-0.1}{=}0.79$
Midplane boundary σ_m	$10^{1.5}{=}31.6$
χ^2	720101
Ring Model	
Fractional abundance	5.5×10^{-11}
R_{out} *(AU)*	*500*
Surface boundary	*T<19 K*
Midplane boundary σ_m	$10^{1.5}{=}31.6$
χ^2	720101

[a]Parameters in italics were fixed from CO modeling (σ_s for the power-law model and R_{out} for the ring model).

Table 3.　Central star and disk, and H_2CO data.

Source	RA	DEC	Spec. type	d [pc]	m_{disk} [$M_\odot$]	Detected H_2CO[i]	Calc. $3_{0,3} - 2_{0,2}$ [Jy km s^{-1}]	T_{rot} [K]
TW Hya[a]	11 01 51.91	−34 42 17.0	K7	56	0.005	$4_{1,4} - 3_{1,3}$, $5_{1,5} - 4_{1,4}$	∼1.3[j]	11(6)
HD 163296[b]	17 56 21.29	−21 57 21.9	A1	122	0.089	$3_{1,2} - 2_{1,1}$, $4_{1,4} - 3_{1,3}$	∼0.46[j]	29(10)
DM Tau[c]	04 33 48.73	+18 10 10.0	M1	140	0.02	$3_{0,3} - 2_{0,2}$, $4_{1,4} - 3_{1,3}$	–	11(4)
AA Tau[c]	04:34:55.42	+24:28:53.2	K7	140	0.01	$3_{0,3} - 2_{0,2}$, $(4_{1,4} - 3_{1,3})$[k]	–	<18
LkCa 15[c]	04 39 17.78	+22 21 03.5	K5	140	0.05	$3_{0,3} - 2_{0,2}$, $4_{1,4} - 3_{1,3}$	–	16(3)
GM Aur[c]	04 55 10.98	+30 21 59.4	K3	140	0.03	$3_{0,3} - 2_{0,2}$, $4_{1,4} - 3_{1,3}$	–	12(5)
IM Lup [d,e]	15 56 09.23	−37 56 05.9	M0	150	0.08	$3_{0,3} - 2_{0,2}$, $4_{1,4} - 3_{1,3}$	–	22(6)
AS 209[f]	16 49 15.29	−14 22 08.6	K5	125	0.028	$3_{0,3} - 2_{0,2}$, $(4_{1,4} - 3_{1,3})$[k]	–	<30
V4046 Sgr[g]	18 14 10.47	−32 47 34.5	K5	73	0.01	$3_{1,2} - 2_{1,1}$, $4_{1,4} - 3_{1,3}$	∼0.92[j]	12(3)
HD 142527[h]	15 56 41.89	−42 19 23.3	F6	145	0.1	$3_{0,3} - 2_{0,2}$, $4_{1,4} - 3_{1,3}$	–	250(120)

Star and disk data from: [a]Qi et al. (2004), [b]Qi et al. (2011), [c]Andrews & Williams (2005), [d]Lombardi et al. (2008), [e]Pinte et al. (2008), [f]Andrews et al. (2009), [g]Rodriguez et al. (2010), [h]Verhoeff et al. (2011). [i]From this work and Öberg et al. (2010, 2011b). Upper limits in parentheses. [j]Calculated from other H_2CO transition strengths and the determined excitation temperature. [k]The $3 - 2$ lines were reported as upper limits in Öberg et al. (2010, 2011b), but after re-examination of the emission maps, we conclude that these lines are better described as tentative detections (2-3σ).